PNAS
www.pnas.org

Supplementary Information for

Catabolism of lysosome-related organelles in color-changing spiders supports intracelullar turnover of pigments

Florent Figon, Ilse Hurbain, Xavier Heiligenstein, Sylvain Trépout, Arnaud Lanoue, Kadda Medjoubi, Andrea Somogyi, Cédric Delevoye, Graça Raposo and Jérôme Casas

Florent Figon and Jérôme Casas
E-mail: florent.figon@univ-tours.fr; jerome.casas@univ-tours.fr

This PDF file includes:

Other supplementary materials for this manuscript include the following:

Supporting Information Text

Materials and Methods

Color Measurements. Body coloration of crab spiders was quantified by measuring reflectance spectra of their integuments as described in (1). For each spider, and time point during the course of color change, color indexes were averaged from three reflectance spectra taken successively. Body coloration was measured the day after capture and no more than a day before processing spiders for further imaging.

Reagents and Solutions. Glucose, Fetal Bovine Serum (FBS), magnesium chloride, sodium chloride and potassium chloride were purchased from Sigma-Aldrich. Uranyl acetate, lead citrate, Durcupan ACM, anhydrous acetone and osmium tetroxide were purchased from EMS.

Transmission Electron Microscopy. Ultra-thin sections (70 nm) were cut with ultramicrotome UCT (Leica Microsystems), stained with uranyl acetate and lead citrate and imaged with a Tecnai Spirit electron microscope (Thermo Fisher Scientific, Netherlands) equipped with à QUEMESA CCD camera (EMSIS) and iTEM software (EMSIS).

Image Analysis and Quantification. The different stages of pigment organelles observable in TEM images were manually contoured in several cells per individual. To calculate the proportions of pigment organelle types, three yellow and three white spiders captured the same day and cryofixed at the same time were used as biological replicates. Proportions were reported as the mean ± standard deviation of the three spiders per color. Morphometric data (maximum Feret diameter as a proxy of size and elongation ratio as a proxy of ellipticity) were automatically computed using Icy software and were reported as the mean ± standard deviation of 666 and 779 organelles observed in the three white and the tree yellow spiders, respectively.

For endogenous metal quantifications, backgrounds of SXRF maps were removed by subtracting to each pixel the average pixel value within a rectangular region comprising only resin using Fiji software (2). Structures positive for osmium were manually selected in the aligned Os maps using round ROIs of 800 nm diameter in Icy software. ROIs were copy-pasted onto endogenous metal maps. Mean pixel values within ROIs were calculated and extracted using Icy software.

Analytical chemistry of pigments. Pigments of a yellow, a white and a one-week bleaching spider were extracted and analyzed using the protocol described in (3). Briefly, acidified methanol was used to extract ommochromes, their precursors and other pigments. Compounds were separated by ultraperformance liquid chromatography with a reversed-phase ACQUITY© system coupled to a photodiode array and a Xevo TQD triple-quadrupole mass spectrometer equipped with an electrospray ionization source (Waters, Millford, MA). Known metabolites of the ommochrome pathway were monitored and quantified using the Multiple Reaction Mode, while unknown metabolites were detected based on their UV-visible absorbance.

Statistical Analysis. All statistical analyses were performed using R software (4). Principal component analyses and hierarchical clustering were done using FactoMineR library. Compositional analyses (ternary plot) of pigment organelle types in color-changing experiments were performed using RobCompositional library. Statistical differences between SXRF populations were tested first by non-parametric Kruskal-Wallis tests and then by pairwise Wilcoxon tests. Only p-values below 0.05 were considered as statistically significant.

Results

Metal Accumulation in Relation to Coloration. We investigated whether the morphological diversity of pigment organelles we described was associated to a variation in metals. First, we compared the distribution of metals in white and yellow integuments using Os as a structural marker of pigment organelles (Fig. S5A and B). Both types of integuments showed high densities of pigment organelles (Os-positive structures) but yellow ones harbored higher amounts of Os (Fig. S5B), in agreement with the presence of more pigmented organelles binding more Os in these tissues. While in white tissues, nuclei accumulate either similar or higher amounts of Zn, Ca and Co than those in yellow tissues (Fig. S5A and B), pigment organelles of yellow tissues accumulate higher amounts of those metals (Fig. S5B). Zn is seemingly present in some pigment organelles of white integuments, albeit in fewer amounts than in yellow tissues. These results suggest that metals are preferentially associated with yellow coloration.

We then investigated whether there was a relationship between pigmentation status at the level of pigment organelles and the presence of metals in yellow integuments. First, we performed correlative STEM-SXRF (Fig S6B-D) that qualitatively showed that more pigmented organelles (b and c types) accumulate more metals (Fig. S5C-D). Next, we quantified the amount of metals within each Os-positive structure of Fig. 4B and we performed a multivariate analysis by principal component analysis (Fig. S5E). The first cluster of pigment organelles was characterized by low concentrations of metals, including Os (Fig. S5F, cluster 1), indicating that the less pigmented organelles (based on Os signal) accumulated less metals. Second and third populations were mostly similar in terms of pigmentation but differed in their concentrations of native metals (Fig. S5F, clusters 2 and 3). Zn, Co and Ca were 1.40, 1.67 and 1.80 times more concentrated, respectively, in population 3 than in population 2.

We then asked whether this heterogeneity in metal distribution was related to morphological diversity. A correlative SXRF-STEM experiment was performed to categorize each Os-positive structure within one of the pigment organelle types described in Fig. 1A. Fig. S5G validates that Os signal recapitulates the pattern of intraluminal density in pigment organelles

as population 1 is enriched in a, d and e types. Populations 2 and 3 do not segregate to distinct morphological types, they are rather enriched in b and c types, as well as in organelles that were intermediate between a and b types. Nonetheless, population 1 is clearly underrepresented in fully pigmented b types (Fig. S5G), which further supports a link between pigmentation status and metals.

Autophagy During Bleaching. Previous studies hypothesized that autophagy fuels the recycling of bleached organelles based on the observation of translucent organelles within swirls of endoplasmic reticulum resembling phagophores (5, 6). We did similar observations (Fig. S12) except that HPF revealed translucent organelles to be lipid droplets and not pigment organelles. Among four spiders, we observed 18 events of ER encircling organelles. The vast majority of these events concerned lipid droplets (9/18) and mitochondria (8/18), but very rarely pigment organelles (1/18), and this even if those cells were enriched in pigment organelles, meaning that the occurrence is rare. Besides, we never observed large fractions of cytoplasm (comprising multiple organelles) engulfed by swirling ER. Similarly, we never observed autophagosomes fusing with lysosomes (to form autolysosomal degradative structures), so we cannot provide evidence that there are autolysosomes among observed lysosomal organelles.

Pigment Catabolism During Bleaching. Pigments produced during yellowing of spiders were investigated by (1), revealing that ommochrome precursors and ommochrome-like pigments were involved. There was however no chemical information on the catabolism of those pigments during bleaching. To provide that information, we applied the analytical method we developed previously on ommochromes of fly eyes (3). We found ommochrome precursors in all spiders, with tryptophan as the main metabolite in the white spider. Kynurenines were more abundant in the yellow and bleaching spiders. We furthermore found xanthommatin and decarboxylated xanthommatin in higher quantities in the yellow spider compared to the bleaching and the white ones (Fig. S10C). This result is consistent with previous publications (1, 7).

We did not observe a "peak" in the three absorbance chromatograms that could be specific to the bleaching spider (Fig. S10A). Yellow spiders seemed to drift to white exclusively through the loss of pigments, without the production of (new) intermediary compounds. Absorbance chromatograms of the yellow and bleaching spiders revealed several peaks absorbing around 370 and 400 nm (i.e. blue region) and thus correspond to yellow pigments (Fig. S10B). Their UV-visible spectrum (Fig. S10B) did not resemble any known pigment. However, the fact that ommochromes precursors (tryptophan and kynurenines) and xanthommatins were present in spiders indicated that those pigments might belong to a still unknown subgroup of ommochromes. Indeed, ommochromes are diverse and comprise at least 3 different subgroups –ommatins, ommins and ommidins– whose structures remain to determine. Furthermore, those unknown pigments we observe do share common characteristics with known ommochromes, such as being soluble in acidified methanol (3).

Discussion

Subcellular Mechanisms of Bleaching in Crab Spiders . The autophagy-like events previously observed in crab spiders using classical TEM (5, 6) proved to be mainly associated to lipid droplets and mitochondria, but not to pigments. Thus, there is no clear link between autophagy and the bleaching process. Furthermore, there is no evidence of autolysosome formation in our data. Since autophagy is a process that can be triggered within a few hours of starvation in cell systems (8) and since it can last over several days leading to bleaching in skin systems (9), we would have expected to observe at least some autophagic events in our study. Indeed, it encompassed spiders bleaching over a few days to weeks and successfully captured events even more rapid than autophagy like membrane tubulations. Based on the lack of evidence, we hypothesize that autophagy is unlikely to be a major contributor to bleaching, although we cannot totally exclude its participation.

Regarding the pigment secretion hypothesis, we never observed pigment organelles in the extracellular space nor their fusion with the plasma membrane, precluding thus their exocytosis.

Chemical Mechanisms of Bleaching. The absence of specific metabolites in bleaching spiders suggests that catabolism is acting through the removal or complete degradation of pigments, and not by a specific catabolic pathway of pigments that would produce metabolites different from the anabolic pathway. This putative mechanism is consistent with the (auto)lysosomal degradation pathway we suggest, which does not require specific metabolic pathways. This would also suggest that pigments are progressively removed from pigment organelles, leaving out the proteinaceous scaffold on which they are deposited (a process similar to the ones observed for melanins), hence explaining the internal morphology of d, e and f types and their putative ordering.

Based on their chemical properties, the biological context and the presence of kynurenines, we suggest that the most reasonable interpretation is that those pigments are ommochrome-like. Verifying this hypothesis would require further chemical studies, however such analytical chemistry would be far beyond the scope of this study as structural elucidation of natural pigments remains a great challenge, requiring both high amounts of materials and dedicated chemical platforms (3, 10, 11). Indeed, we only last year identified a precursor at the root of the entire ommochrome pathways due to its unstable and transient nature, as well as the delicate chemistry required for extracting intact pigment organelles (3).

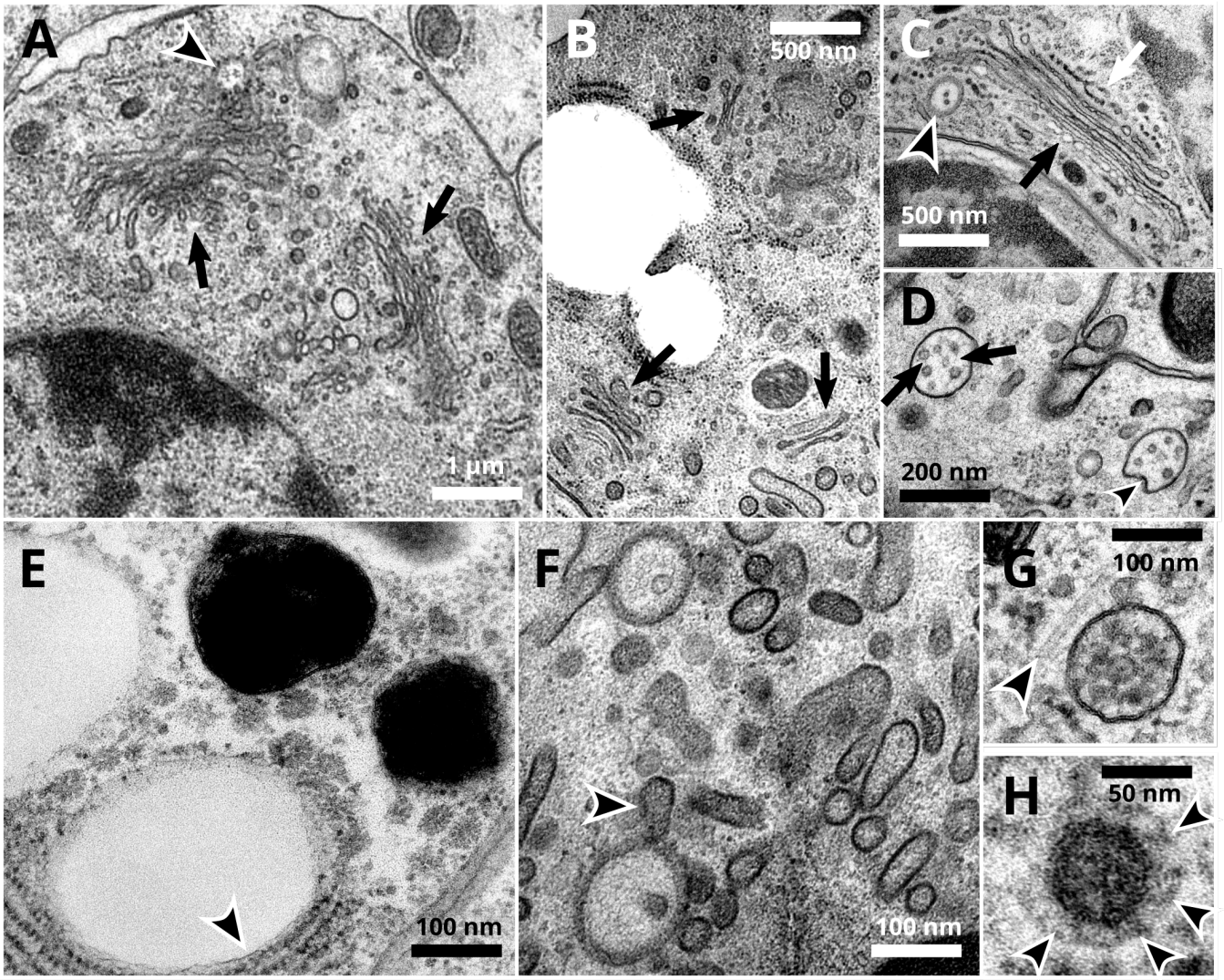

Fig. S1. Ultrastructure of crab spider cells preserved by high-pressure freezing and freeze substitution. (A) A non-pigment cell showing well-preserved nucleus, mitochondria, Golgi apparatus with clear stacked structures and budding profiles (arrows) and a closely associated endosome (arrowhead). (B) Multiple Golgi apparatus (arrows) with neat stacked structures within a non-pigment cell. (C) A stacked and budding Golgi apparatus showing distinct cis- (white arrow) and trans- (black arrow) sides in a non-pigment cell. An endosome harboring intraluminal vesicles (arrowhead) is closely associated. (D) Two endosomal compartments with multiple intraluminal vesicles (ILVs) and fibrils (arrows). The limiting membrane of one of these endosomal compartments is budding inward (arrowhead), likely forming a new ILV. (E) A lipid droplet closely associated to endoplasmic reticulum (arrowhead). (F) Endosomes and tubules within a non-pigment cell. An endosome display a tubulating membrane (arrowhead). (G) A microtubule (arrowheads pointing to its ends) closely associated to cytosolic vesicles and to a budding multivesicular body. (H) A cytosolic vesicle displaying a coat of proteins (arrowhead) resembling clathrin.

Florent Figon, Ilse Hurbain, Xavier Heiligenstein, Sylvain Trépout, Arnaud Lanoue, Kadda Medjoubi, Andrea Somogyi, Cédric Delevoye, Graça Raposo and Jérôme Casas

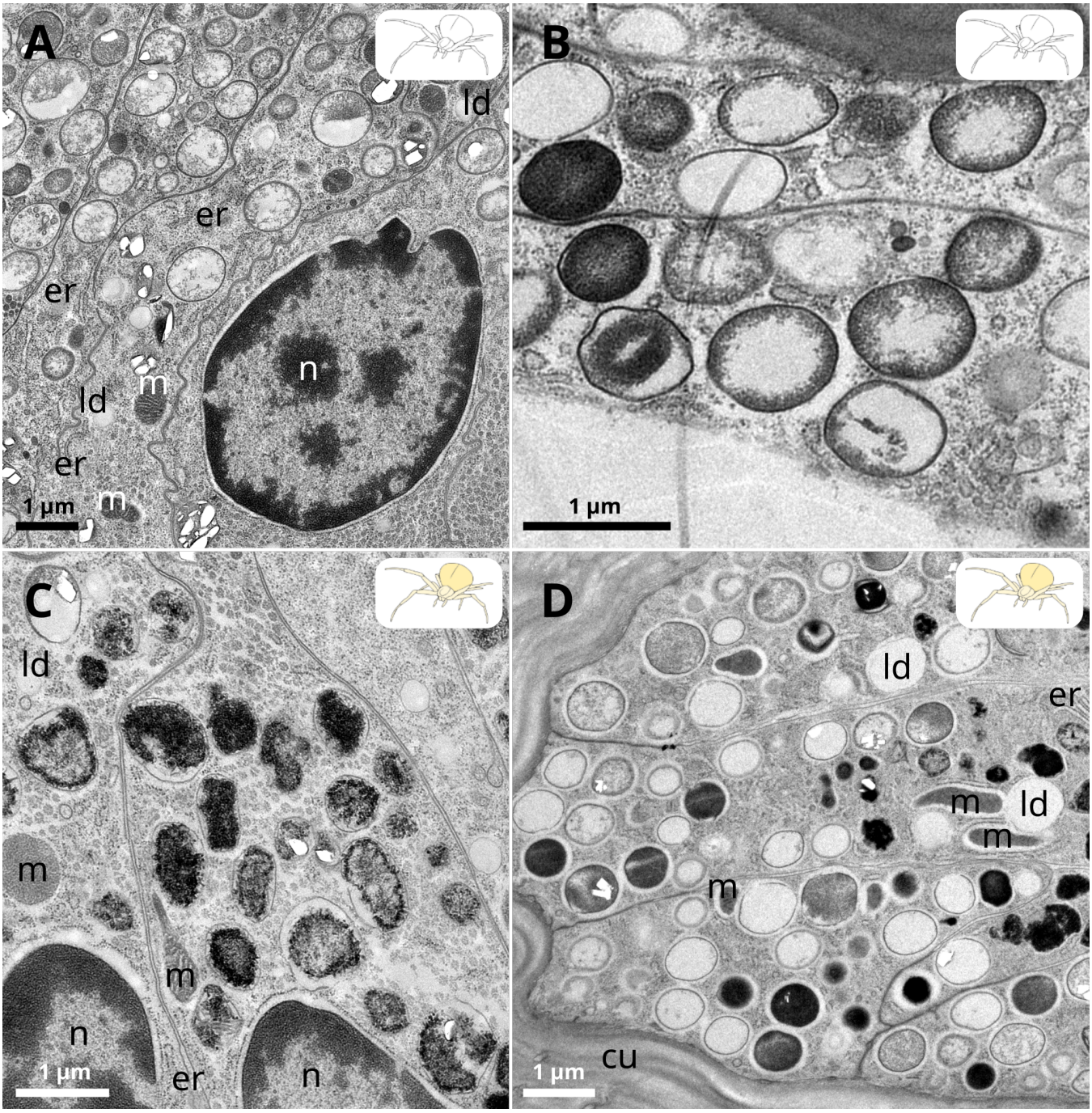

Fig. S2. Ultrastructural diversity of pigment organelles. (A) Early stages of pigment organelles in a white crab spider. (B) Pigment organelles at different stages of filling in a white spider. (C) Pigment organelles observed only in a yellow crab spider. (D) Variety of pigment organelles observed in yellow spiders. cu, cuticle; er, endoplasmic reticulum; ld, lipid droplet; m, mitochondria; n, nucleus.

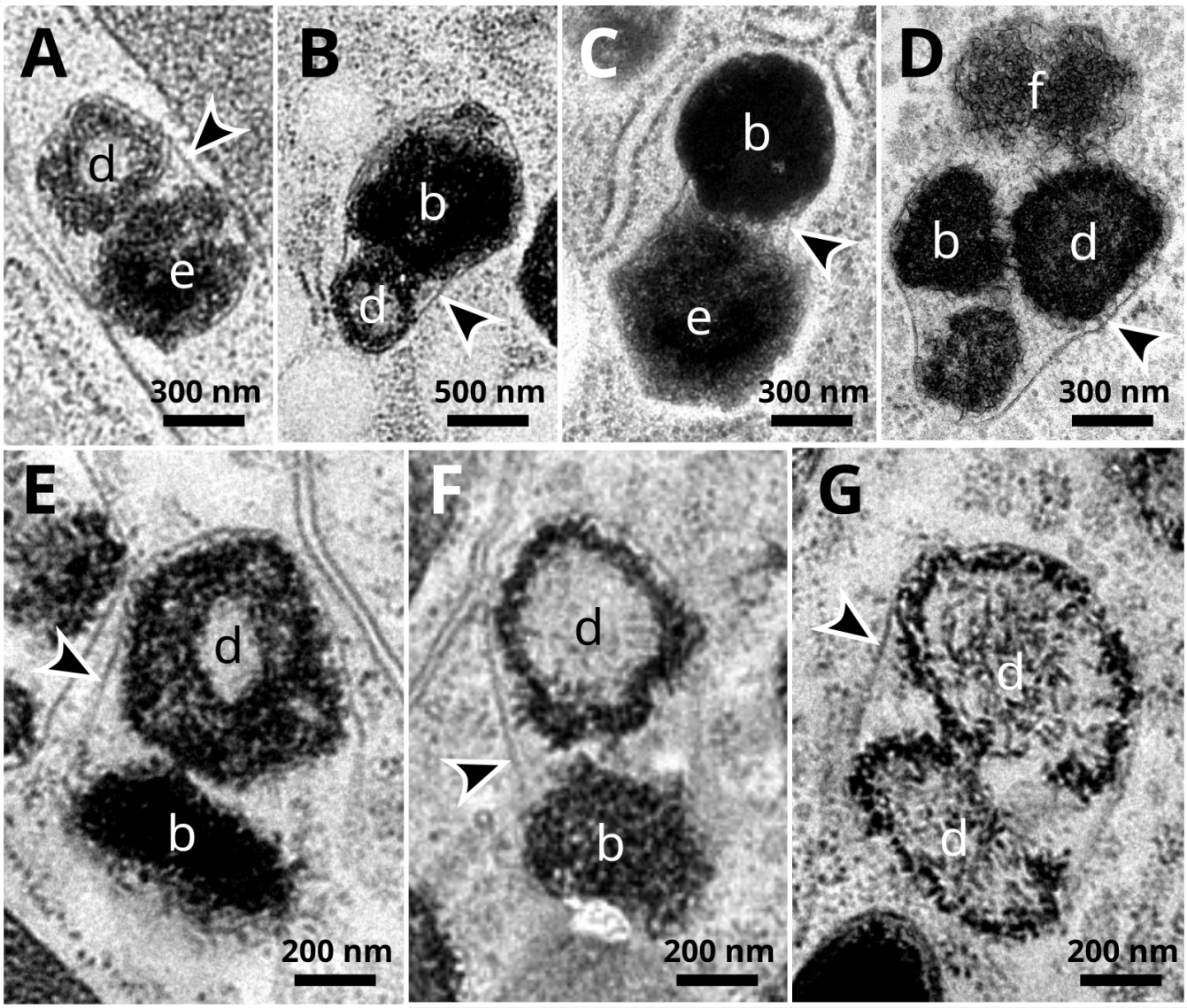

Fig. S3. Various pigment organelle types observed within c-type clusters. (A-G) The various types of pigment organelles recognizable within c-type clusters are indicated by their respective letters. All c types possess a single limiting membrane (arrowheads).

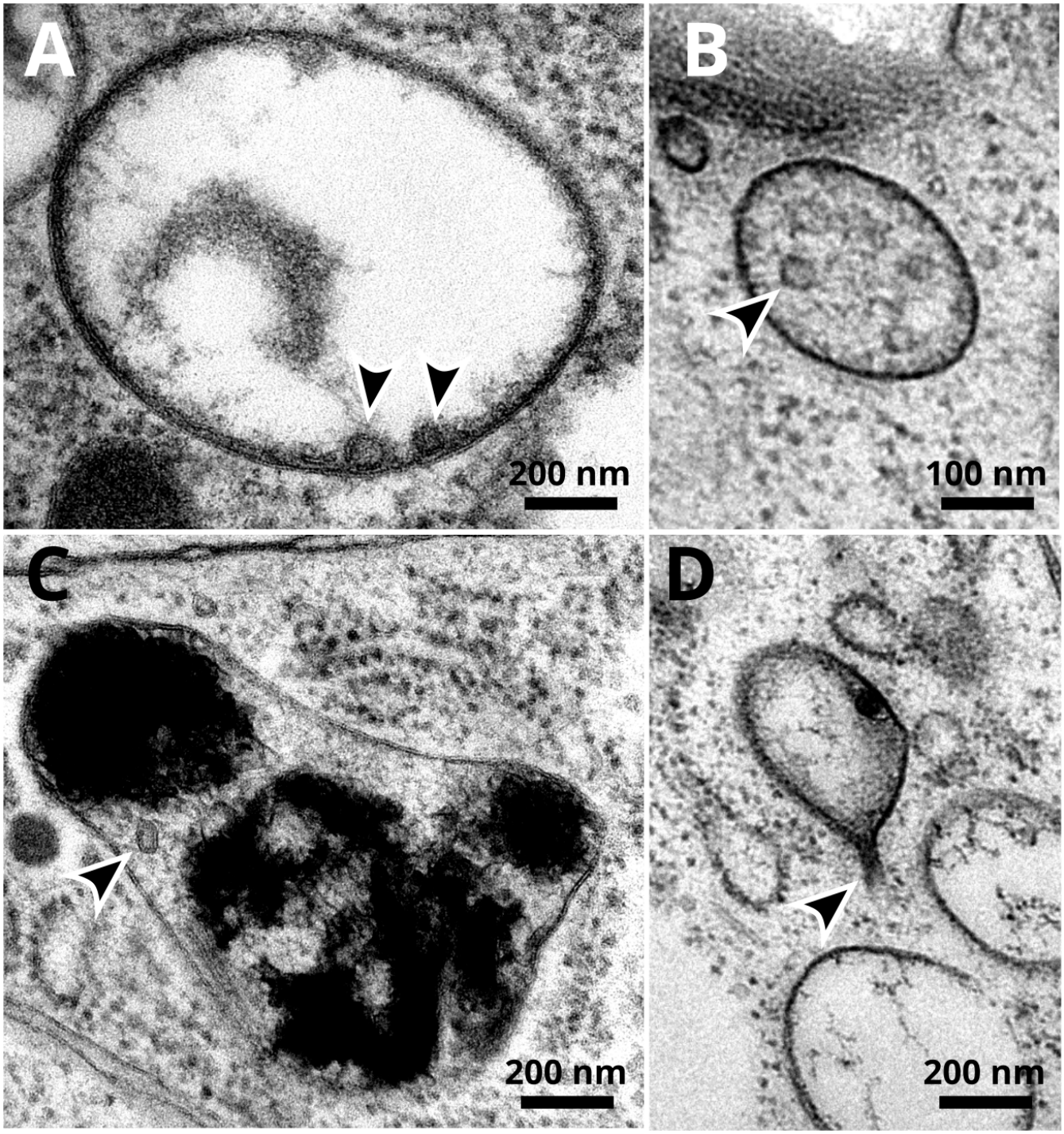

Fig. S4. Intraluminal vesicles and membrane tubulations of pigment organelles. (A) Two intaluminal vesicles (arrowheads) closely associated to the limiting membrane of an early a-type pigment organelle. (B) Intraluminal vesicles and fibrils in a multivesicular body resembling a maturating a-type pigment organelle. (C) A intraluminal vesicle (arrowhead) within a c-type cluster of pigment organelles. (D) Tubulation of the limiting membrane (arrowhead pointing toward the tubule neck) of an early a-type pigment organelle.

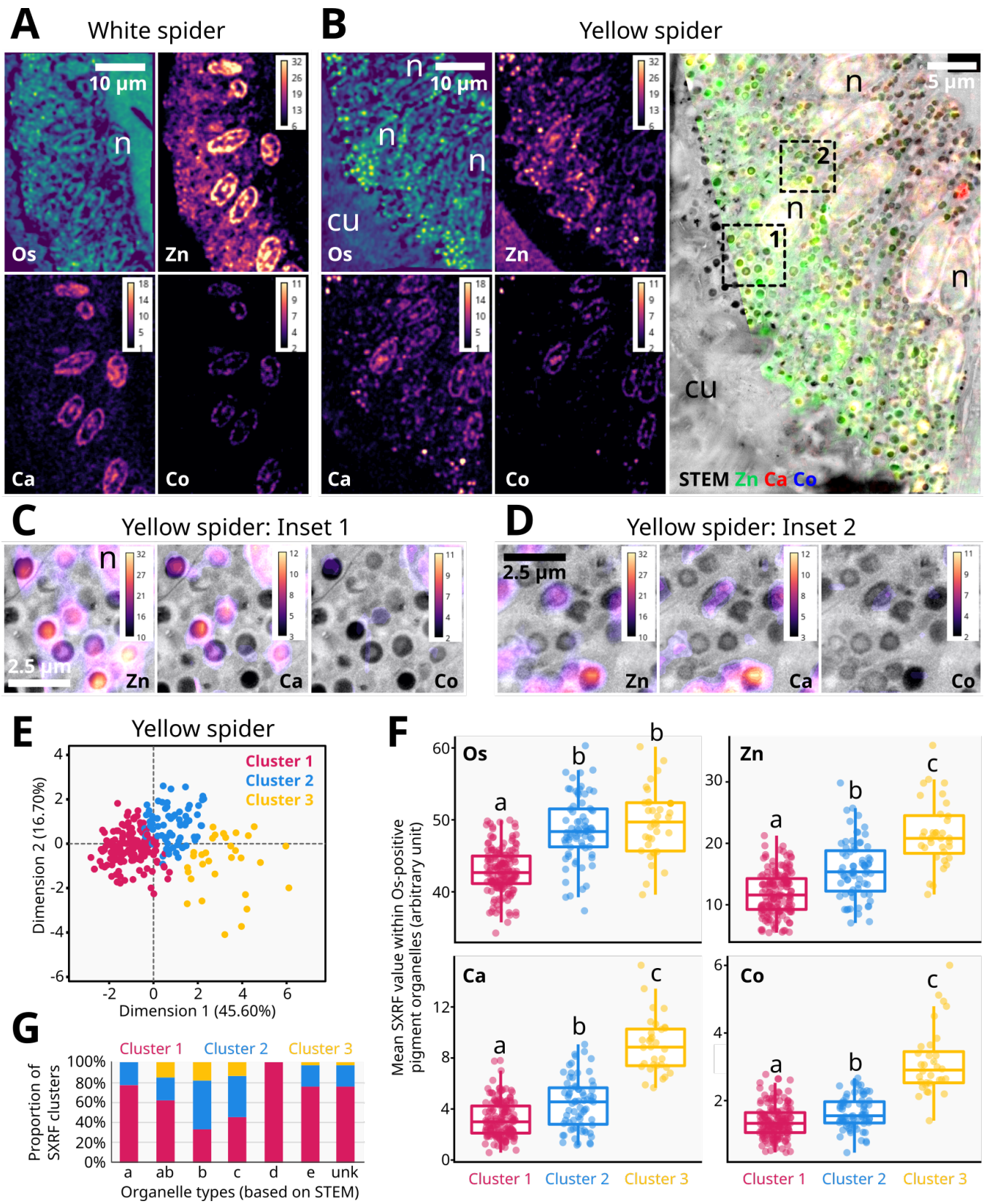

Fig. S5. Pigment organelles differentially accumulate metals according to coloration and maturation stages. (A-B) Synchrotron X-ray fluorescence (SXRF) mapping of osmium (Os) and native zinc (Zn), calcium (Ca) and cobalt (Co) in white (A) and yellow (B) integuments. A correlative SXRF-STEM imaging of the yellow integument is provided. cu, cuticle; n, nucleus. (C-D) Zoom of the two regions depicted in B. (E) Principal component analysis and hierarchical clustering of Os-positive organelles in B based on their average content in Os, Zn, Ca, Co, S and Ni. (F) Metal contents in the clusters depicted in E. (G) Relative abundance of SXRF clusters defined in E according to organelle types. Different letters indicate statistical significance between clusters (p-value < 0.05; Kruskal-Wallis test followed by pairwise Wilcoxon rank sum test using Holm method for p-value adjustment). ab, pigment organelles with an intermediary morphology between a and b types; Unk, unknown organelles whose ultrastructure by STEM was too ambiguous to be classified.

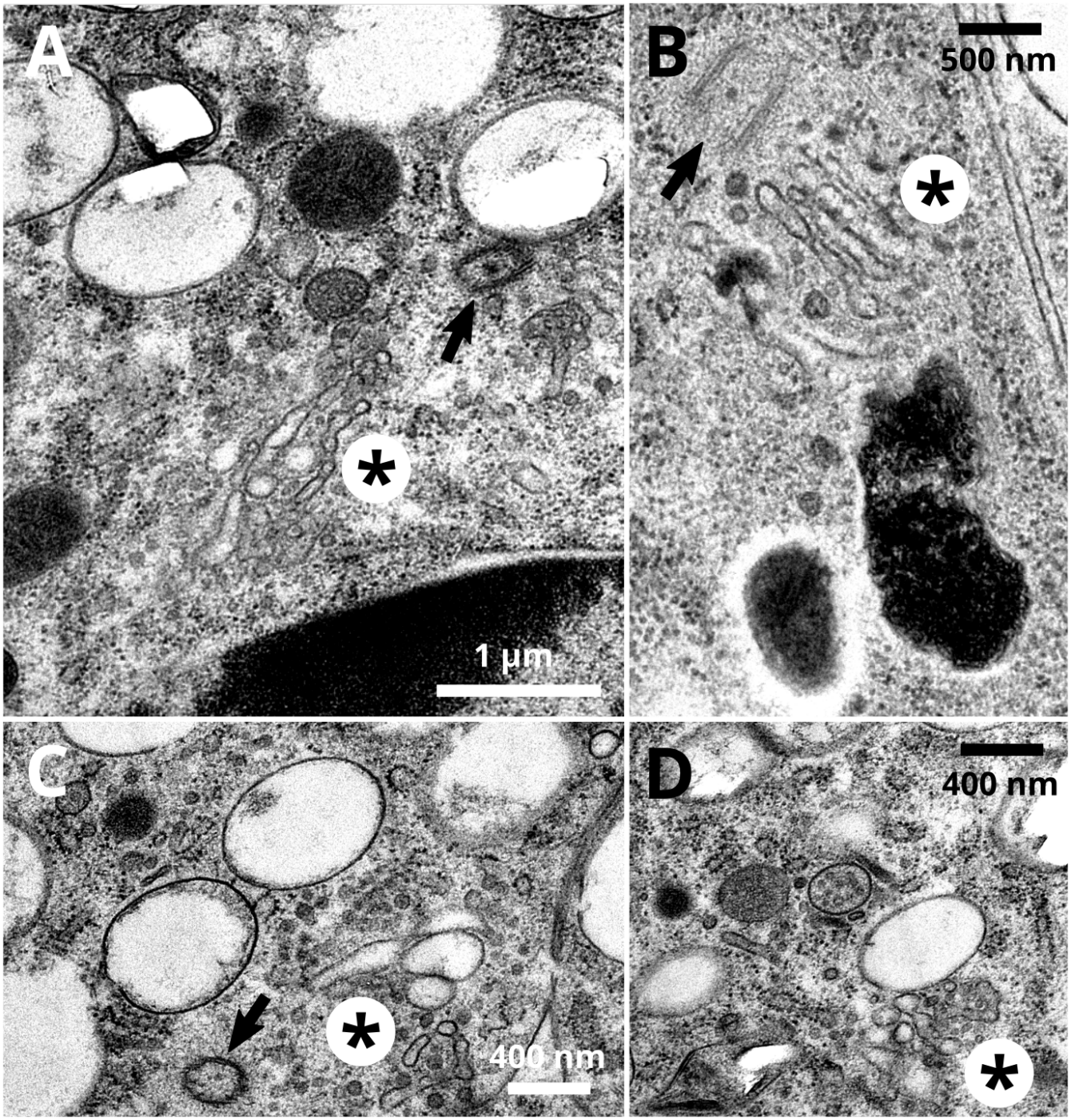

Fig. S6. Examples of tubulosaccular complexes in pigment cells of crab spiders. (A-C) Centrioles (arrows) can be observed in regions where tubulosaccular complexes (asterisk) are situated. (D) Another example of a tubulosaccular complex closely associated to an early a-type pigment organelle, endosomal compartments, vesicles and tubules.

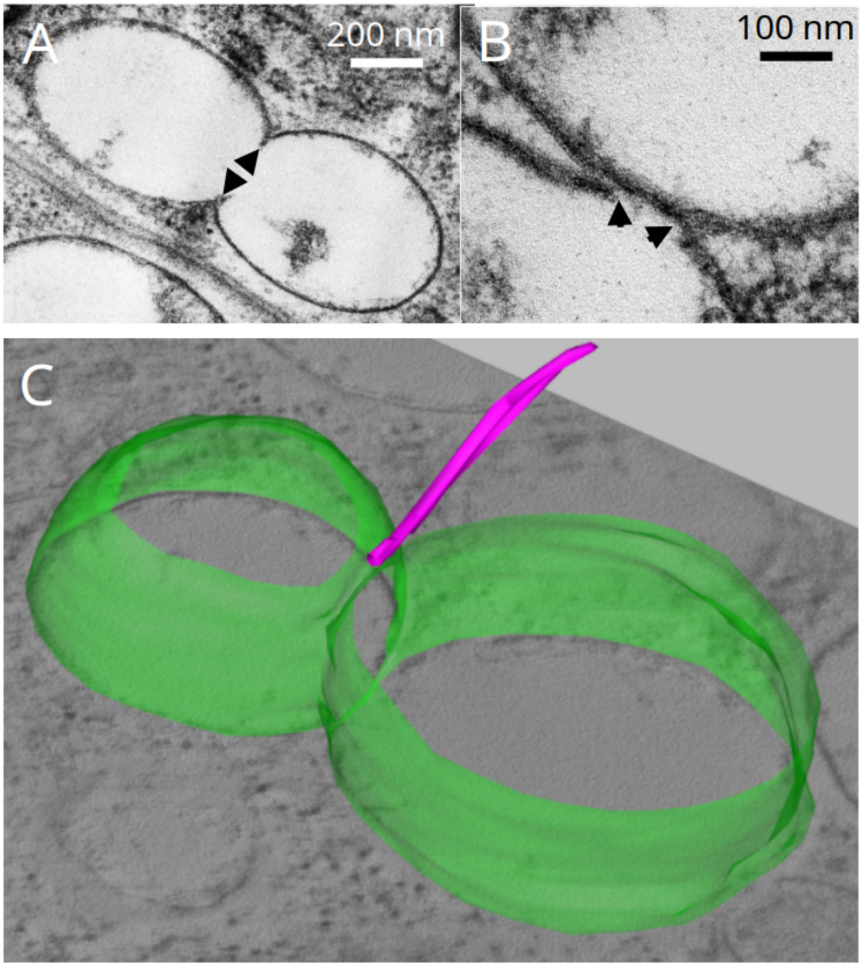

Fig. S7. Evidence of homotypic fusion events between a-type pigment organelles in white spiders. (A-B) Continuity of limiting membranes (arrowheads) suggest homotypic fusion events between a-type pigment organelles. (C) Three-dimensional reconstruction of fused a-type pigment organelles (green membrane) showing a microtubule (magenta) closely-associated to the fusion site.

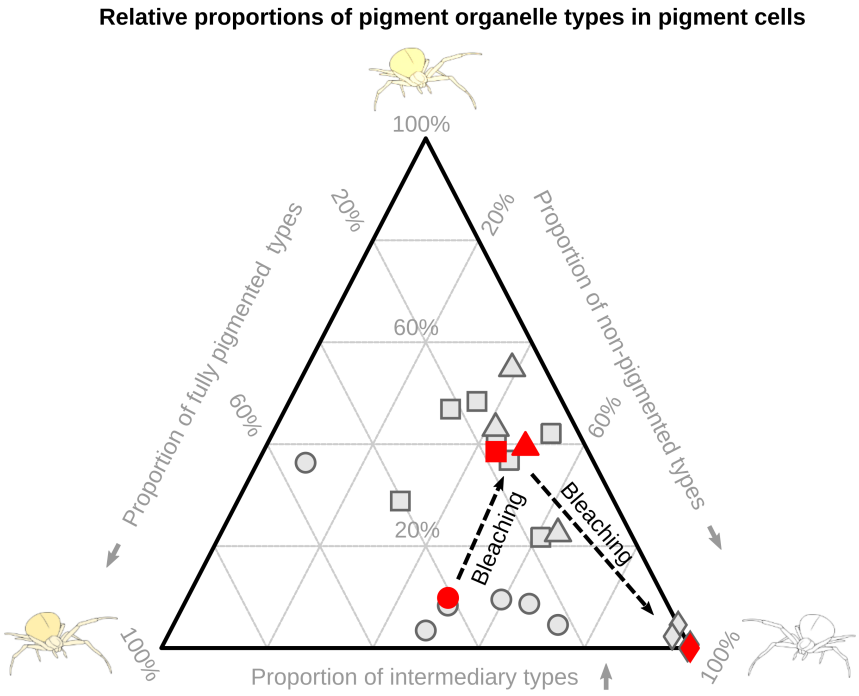

Fig. S8. Ternary plot of the proportions in pigment organelle types for four bleaching spiders. Circle, unbleached yellow spider; triangle, bleaching spider; square, more advanced bleaching spider; diamond, fully bleached white spider; see Materials and Methods. Between three to seven cells (grey symbols) were analyzed per individual. Geometric, rather than arithmetic, means (red symbols) were computed to preserve ratios between pigment organelle types. Intermediary types, c, d, e and f types; Non-pigmented types, a types; Pigmented types, b types.

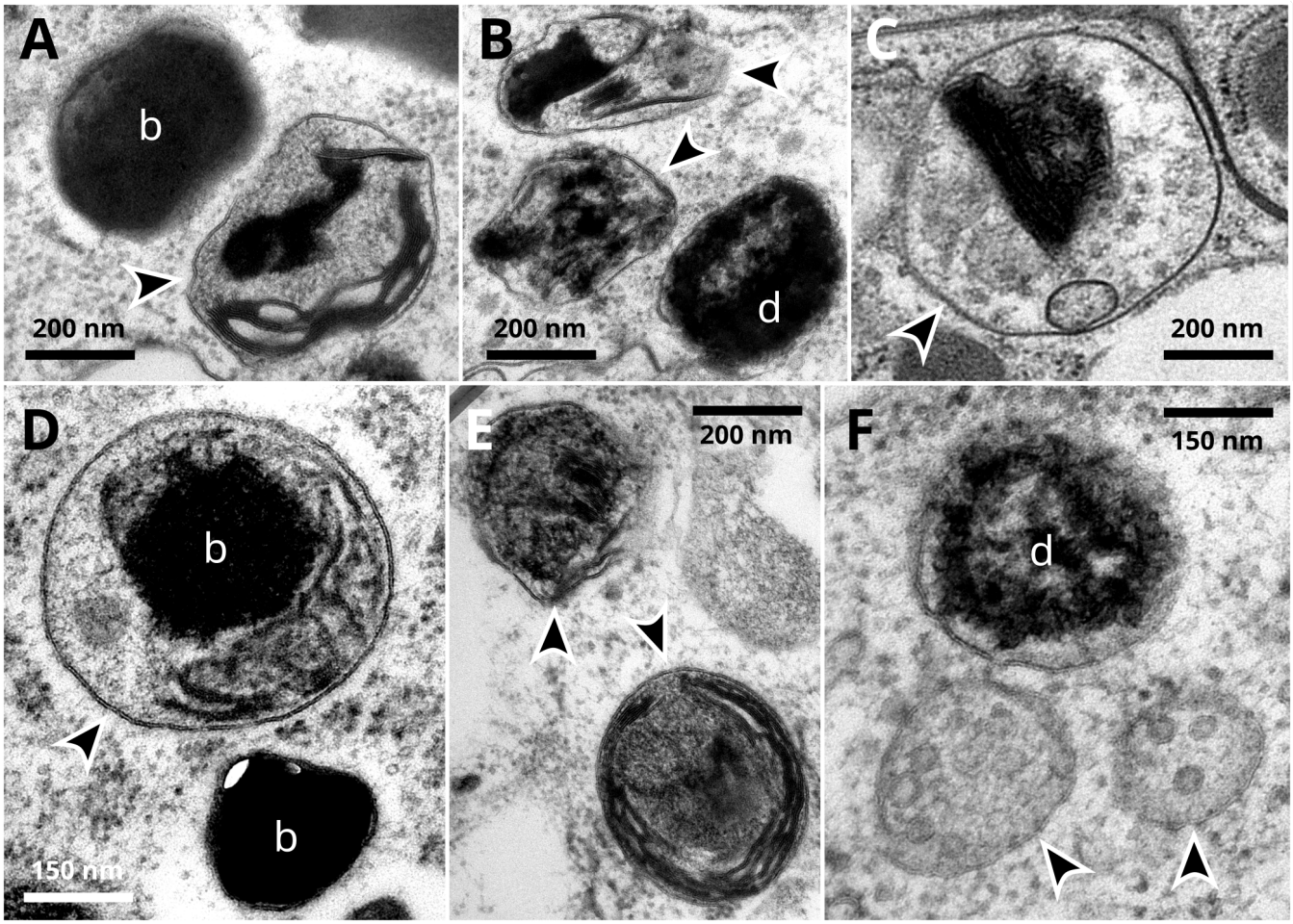

Fig. S9. Ultrastructural evidence of lysosomal degradation of pigment organelles. (A-E) Lysosomal compartments (arrowheads) displaying a single limiting-membrane, dense lumens, heterogeneous and aggregated materials, as well as cores of b-type pigment organelles are observed, sometimes in the close vicinity of free pigment organelles. (F) Two multivesicular bodies (arrowheads) with dense granular lumens resembling late endosomes are closely associated to a d-type pigment organelle.

Florent Figon, Ilse Hurbain, Xavier Heiligenstein, Sylvain Trépout, Arnaud Lanoue, Kadda Medjoubi, Andrea Somogyi, Cédric Delevoye, Graça Raposo and Jérôme Casas

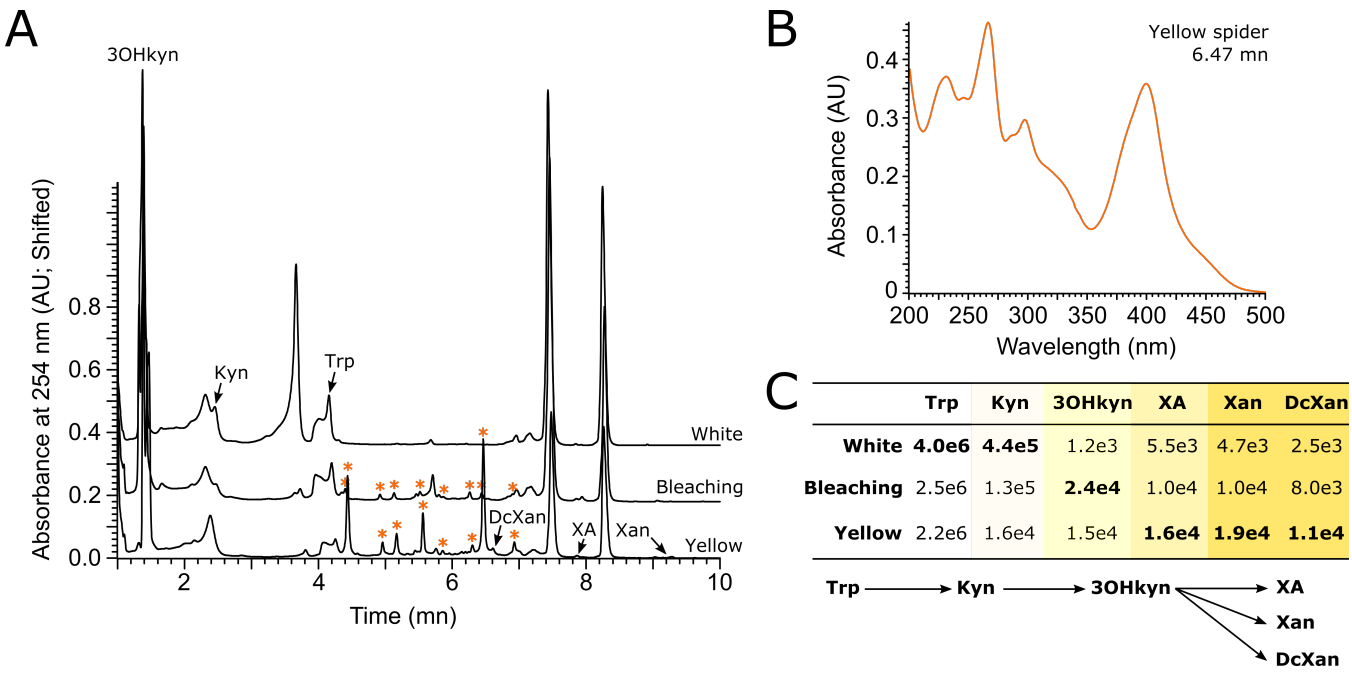

	Trp	Kyn	3OHkyn	XA	Xan	DcXan
White	**4.0e6**	**4.4e5**	1.2e3	5.5e3	4.7e3	2.5e3
Bleaching	2.5e6	1.3e5	**2.4e4**	1.0e4	1.0e4	8.0e3
Yellow	2.2e6	1.6e4	1.5e4	**1.6e4**	**1.9e4**	**1.1e4**

Fig. S10. Analytical chemistry of pigment extract from a bright white, a bleaching and a bright yellow crab spider. A) Absorbance chromatogram of acidified methanol extracts. Stars denote pigments specific to both yellow and bleaching spiders and that display the absorbance spectrum shown in B. The bleaching spider shows lower peaks than the yellow one. B) Absorbance spectrum of an unknown pigment extracted from the yellow spider, tentatively identified as ommochrome-like. The peak at 400 nm (purple/blue region of visible light) indicates that it is a yellow pigment. C) Quantification by MRM (multiple reaction mode) of ommochrome metabolites detected in mass chromatograms of acidified extracts. Quantification corresponds to peak area (arbitrary unit). Background colors are indicative of each metabolite hue in solution. The highest value for each metabolite is indicated in bold font. The ommochrome pathway is depicted beneath the table. 3OHKyn, 3-hydroxykynurenine; DcXan, decarboxylated xanthommatin; Kyn, kynurenine; Trp, tryptophan; XA, xanthurenic acid; Xan, xanthommatin.

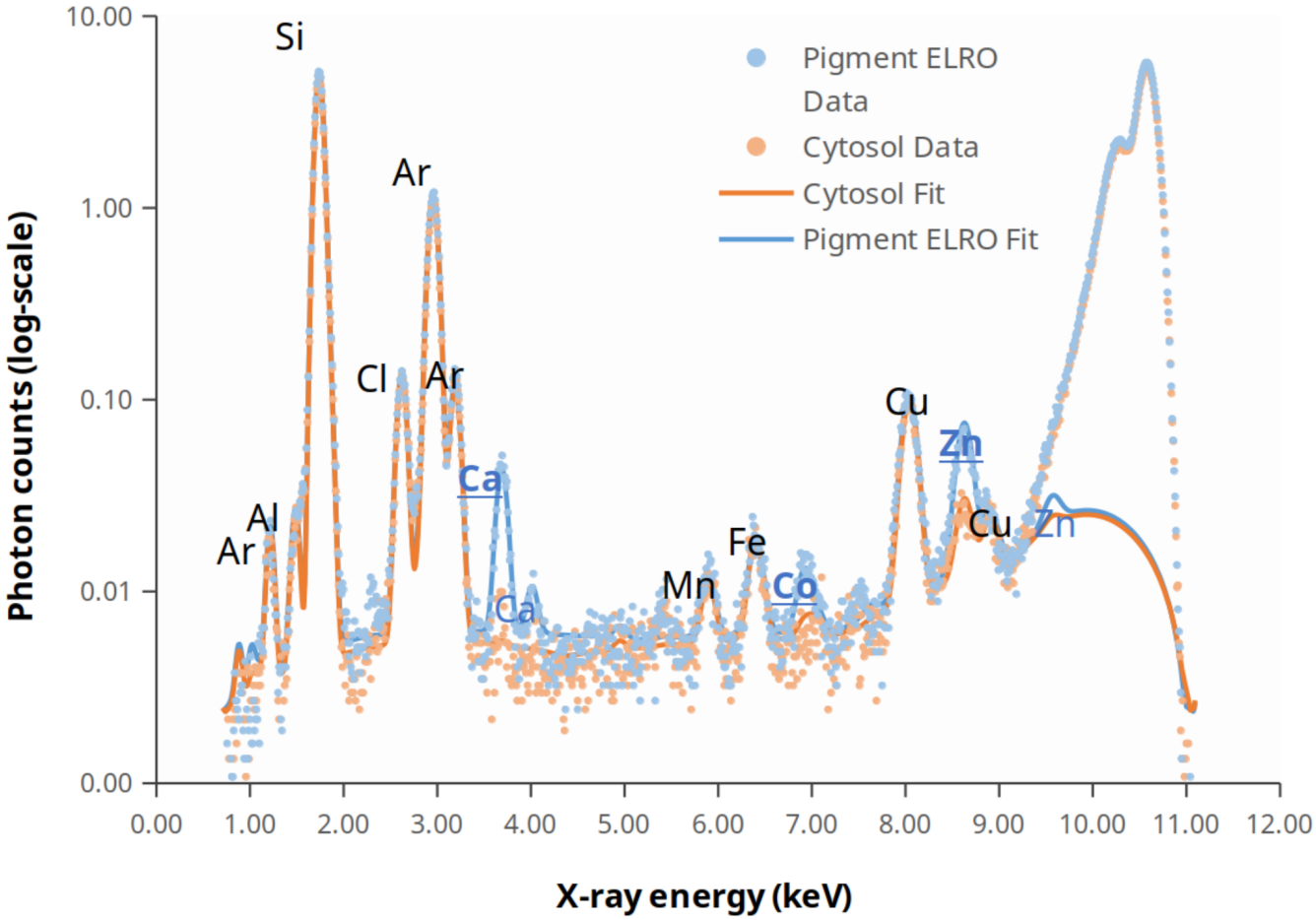

Fig. S11. Recorded Synchrotron X-ray spectra of two intracellular regions within the same cell. X-ray fluorescence of native metals were obtained by exciting the area shown in the inset Figure 3C, which contains a single pigment organelle surrounded by cytosol. Recorded data are displayed as dots. Main fluorescence peaks (K-lines) of elements between Al and Zn are shown as continuous lines. X-ray energies above 9.7 keV are dominated by scattered X-rays. Elements indicated in blue fonts (Ca, Co and Zn) are those with higher fluorescence in the pigment organelle than in the cytosol. The peaks of underlined elements are those used for metal mappings in this study.

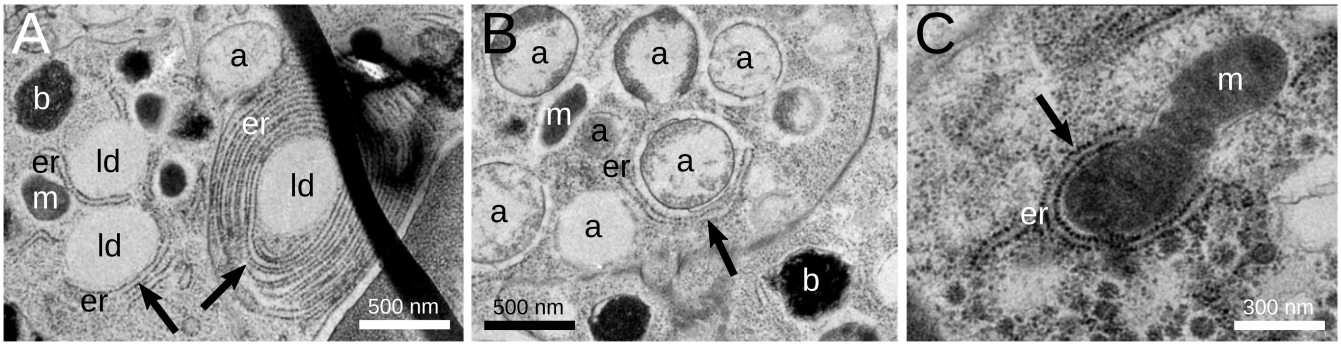

Fig. S12. Examples of autophagy-like events involving endoplasmic reticulum circling organelles (arrows), such as lipid droplets (A), pigment organelle (B) and mitochondria (C). a, a-type pigment organelle; b, b-type pigment organelle; er, endoplasmic reticulim; m, mitochondria; ld, lipid droplet.

Table S1. Characteristics of pigment organelle types in white (W) and yellow (Y) spiders (mean ± SD)

Pigment organelle type	a	b	c	d	e	f
Proportion of all pigment organelles	97 ± 4% (W[a])	3 ± 4% (W)	0% (W)	0% (W)	0% (W)	0% (W)
	11 ± 9% (Y[b])	41 ± 26% (Y)	11 ± 2% (Y)	25 ± 11% (Y)	4 ± 3% (Y)	8 ± 7% (Y)
Size[c] (µm)	0.73 ± 0.19 (W)	0.55 ± 0.10 (W)	N.D. (W)	N.D. (W)	N.D. (W)	N.D. (W)
	0.84 ± 0.25 (Y)	0.75 ± 0.16 (Y)	0.95 ± 0.19 (Y)	0.75 ± 0.15 (Y)	0.74 ± 0.15 (Y)	0.70 ± 0.17 (Y)
Ellipticity[d]	1.37 ± 0.19 (W)	1.25 ± 0.16 (W)	N.D. (W)	N.D. (W)	N.D. (W)	N.D. (W)
	1.38 ± 0.17 (Y)	1.30 ± 0.19 (Y)	1.55 ± 0.33 (Y)	1.31 ± 0.21 (Y)	1.29 ± 0.17 (Y)	1.31 ± 0.16 (Y)

[a] Total of 666 pigment organelles in N = 3 white spiders
[b] Total of 779 pigment organelles in N = 3 yellow spiders
[c] Maximum Feret diameter
[d] Elongation ratio

Movie S1. Tomographic reconstruction of a pigment organelle showing intraluminal vesicles (in blue) and sheet-like fibrils (in gold) associated to the limiting membrane (in green).

Movie S2. Tomographic reconstruction of a c-type pigment organelle showing several cores of intraluminal content (in gold) and two tubulations of the limiting membrane (in green).

Movie S3. Tomographic reconstruction of a tubulosaccular complex (limiting membranes in various colors and intraluminal fibrillary content in gold) and its associated organelles, including free vesicles and tubules (in magenta), a-type pigment organelles (limiting membrane in green and intraluminal fibrillary content in gold) and an endosome (limiting membrane in purple and intraluminal vesicles in blue).

Movie S4. Tomographic reconstruction of the endosome (in purple) observed in Movie S3, displaying intraluminal vesicles (in blue) and a membrane tubulation.

Movie S5. Tomographic reconstruction of a d-type pigment organelle and its intraluminal content (in gold) displaying a pillar-like structure connecting the limiting membrane (in green).

Movie S6. Tomographic reconstruction of a f-type pigment organelle and its intraluminal content (in gold) showing its intertwined sheet-like structure.

Movie S7. Tomographic reconstruction of a c-type pigment organelle and its intraluminal content (in gold) displaying a pillar-like structure that connects its two cores.

References

1. A Llandres, F Figon, JP Christides, N Mandon, J Casas, Environmental and hormonal factors controlling reversible colour change in crab spiders. *J. Exp. Biol.* **216**, 3886–3895 (2013).
2. J Schindelin, et al., Fiji: an open-source platform for biological-image analysis. *Nat. Methods* **9**, 676–682 (2012).
3. F Figon, et al., Uncyclized xanthommatin is a key ommochrome intermediate in invertebrate coloration. *Insect Biochem. Mol. Biol.* **124**, 103403 (2020).
4. R Core Team, *R: A Language and Environment for Statistical Computing*. (R Foundation for Statistical Computing, Vienna, Austria), (2017).
5. T Insausti, J Casas, The functional morphology of color changing in a spider: Development of ommochrome pigment granules. *J. Exp. Biol.* **211**, 780–789 (2008).
6. T Insausti, J Casas, Turnover of pigment granules: Cyclic catabolism and anabolism of ommochromes within epidermal cells. *Tissue Cell* **41**, 421–429 (2009).
7. M Riou, JP Christidès, Cryptic Color Change in a Crab Spider (Misumena vatia): Identification and Quantification of Precursors and Ommochrome Pigments by HPLC. *J. Chem. Ecol.* **36**, 412–423 (2010).
8. S Kimura, T Noda, T Yoshimori, Dissection of the Autophagosome Maturation Process by a Novel Reporter Protein, Tandem Fluorescent-Tagged LC3. *Autophagy* **3**, 452–460 (2007).
9. D Murase, et al., Autophagy has a significant role in determining skin color by regulating melanosome degradation in keratinocytes. *J. Investig. Dermatol.* **133**, 2416–2424 (2013).
10. H Berland, et al., Auronidins are a previously unreported class of flavonoid pigments that challenges when anthocyanin biosynthesis evolved in plants. *Proc. Natl. Acad. Sci.* **116**, 20232–20239 (2019).
11. PR Denish, et al., Discovery of a natural cyan blue: A unique food-sourced anthocyanin could replace synthetic brilliant blue. *Sci. Adv.* **7**, eabe7871 (2021).